

Microstrip antennas

R. CHATTERJEE AND N. S. GANESAN*

Electrical Communication Engineering Department, Indian Institute of Science, Bangalore 560 012.

Received on June 11, 1979.

Abstract

Analysis of near field, calculation of radiation pattern using the method of angular spectrum of plane waves, study of input impedance, gain, radiation efficiency as function of substrate thickness and strip widths of microstrip antennas excited at TM_{mn}^z mode at X-band form the subject-matter of the present paper.

Key words : Radiation pattern, microstrip antennas, angular spectrum, Principle of images.

1. Introduction

Extensive theoretical studies of microstrips operating in quasi-TEM mode have been made by several authors with a view to develop microstrip components. Lewin¹ proposed a method of calculating the radiation from strip lines of small spacing. Denlinger², Munson³ and Howell⁴ have also studied radiation problems of microstrip antenna. The authors have recently reported^{5,6} a new line of approach for calculating radiation characteristics of microstrip antennas.

The primary object is to present a new theory based on the concept of angular spectrum of plane waves and the principle of images for the radiation characteristics of microstrip antennas excited in TM_{mn}^z mode and its verification by experiment.

2. Analysis of near field

Analysis of near field will justify the feasibility of exciting TM_{mn}^z mode associated with the non-existence of quasi-TEM mode.

* Presently with the British Physical Laboratories (BPL), Bangalore.

2.1. Geometry of the microstrip

The geometry of the microstrip structure and the cross-sectional view indicating three regions are shown in Fig. 1a and 1b respectively.

2.2. Field distributions

The coaxial-line method of excitation of TM_{zmn}^e which is also the method for exciting quasi-TEM and the field distributions are shown in Figs. 2 and 3 respectively.

The wave equation⁷

$$\nabla_z^2 \phi + (\epsilon_r k^2 - \beta^2) \phi = 0 \quad (1)$$

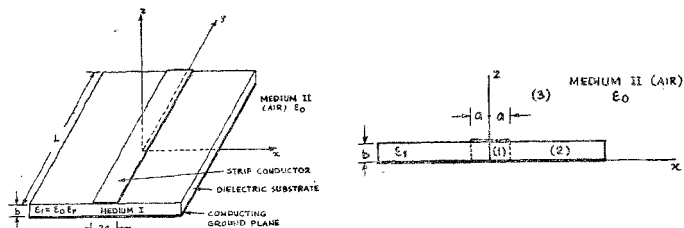


FIG. 1 (a). Geometry of microstrip. FIG. 1 (b). Cross-section of microstrip showing the regions (1), (2) and (3).

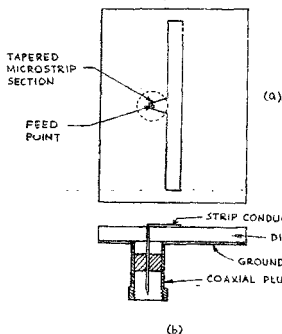


FIG. 2. Excitation mechanism for the microstrip structure. (a) Plan, (b) Sectional view.

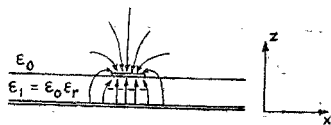


FIG. 3. Cross-sectional view of the microstrip structure showing the field lines.
 ——— Electric field lines.
 - - - - Magnetic field lines.

which reduces to

$$\nabla_z^2 \phi + (k^2 - \beta^2) \phi = 0 \text{ for } \epsilon_r = 1 \quad (2)$$

which further reduces to Laplace's equation

$$\nabla_z^2 \phi = 0 \quad \text{for } k = \beta \quad (3)$$

involves the wave number k in the substrate of dielectric constant ϵ_r and scalar potential ϕ . The wave equation for which $\epsilon_r \neq 1$ characterises quasi-TEM mode only when k is very small, *i.e.*, quasi-TEM mode can exist only at low frequencies. For X-band operation, quasi-TEM mode can exist if the substrate thickness⁸ $\ll 0.8$ mm. The substrate thickness used in the present investigations varies from 2 to 12 mm which is much greater than $0.03 \lambda_0$ suggested by Weiss⁹. For large substrate thickness the microstrip behaves like a grounded dielectric sheet¹⁰ and can support either TM or TE or both depending on the method of excitation but not quasi-TEM mode.

All the field components for the TM_{mn}^z mode are derivable from a scalar potential

$$\begin{aligned} E_x &= \frac{i}{\omega \epsilon} \frac{\partial^2 \psi}{\partial x \partial z} & ; & \quad H_x = -\frac{\partial \psi}{\partial y} \\ E_y &= \frac{i}{\omega \epsilon} \frac{\partial^2 \psi}{\partial y \partial z} & ; & \quad H_y = \frac{\partial \psi}{\partial x} \\ E_z &= \frac{i}{\omega \epsilon} \left(\frac{\partial^2}{\partial z^2} + k_0^2 \epsilon_r \right) \psi & ; & \quad H_z = 0 \end{aligned} \quad (4)$$

where the time dependence $\exp(-i\omega t)$ is omitted for the sake of convenience and $k_0 = \omega(\mu_0 \epsilon_0)^{1/2} = 2\pi/\lambda_0$ the wave number in free space.

2.3. The scalar potential

The microstrip guide can be considered to be analogous to a parallel plate waveguide filled with a homogeneous dielectric of dielectric constant ϵ_r . The modal distribution for TM_{mn}^z mode is represented by a scalar potential

$$\psi_{mn} = \exp(-i a_m x) \exp(i \beta_{mn} y) \cos \frac{n\pi z}{b} \quad (5)$$

where a_m and β_{mn} denote, respectively, the propagation constants along the x and y directions.

In the microstrip guide a standing wave is set up between the ground plane and the strip in the z -direction. Hence the wave proceeding in the x -direction is reflected at $x = \pm a$ due to the finite size of the strip, thus setting up a standing wave also in the x -direction. Consequently eqn. 5 is modified to

$$\begin{aligned} \psi_{m,n} &= [\exp(-i a_m x) + R_{mn} \exp(i 2a_m a) \exp(i a_m x)] \\ &\quad \times \exp(i \beta_{mn} y) \cos(n\pi z/b) \end{aligned} \quad (6)$$

where R_{mn} denotes the reflection coefficient at $x = \pm a$. If $|R_{mn}| = 1$, a resonance condition is set up in region 1, bounded by the ground plane and the strip if the following condition¹⁰ is satisfied.

$$R_{mn} \exp(i 2\alpha_m a) = \exp[i(m+1)\pi]; \quad m = 1, 2 \quad (7)$$

which yields the propagation constant a in the x -direction

$$\alpha_m = \frac{m\pi}{2a} + i \frac{1}{2a} \ln(-R_{mn}) \quad (8)$$

which is satisfied if the wave impedances in the two regions 1 and 2 are very much different, *i.e.*, the discontinuity at $x = \pm a$ is appreciable so as to make $|R_{mn}| = 1$. The propagation constants α_m and β_{mn} satisfy the dispersion relation

$$\beta_{mn} = \left[k_0^2 \epsilon_r - \alpha_m^2 - \left(\frac{n\pi}{b} \right)^2 \right]^{1/2} \quad (9)$$

2.3.1. Estimation of R_{mn}

The value of $|R_{mn}|$ is assumed arbitrarily in the range 1.0 to 0.001 in steps of 0.001, R_{mn} is of the form $(R_1 + iR_2)$ with $R_1 = R_2$. α_m is calculated (eqn. 8) for each value of R_{mn} . The process is repeated for several modes $m, n = (1, 1); (2, 1); (1, 2); (2, 2)$. β_{mn} is then calculated (eqn. 9). The guide wavelength λ_g is given by

$$\lambda_g = \frac{2\pi}{\text{Re}(\beta_{mn})} \quad (10)$$

The calculations for α_m, β_{mn} and λ_g made for microstrips (see Appendix I, for specifications) are reported in Appendix II.

2.3.2. Determination of R_{mn} by a rigorous analytical method

R_{mn} determined¹⁰ by using Wiener-Hopf technique is given by

$$R_{mn} = [\alpha_m + (k_0^2 \epsilon_r - \beta_{mn}^2)^{1/2}]^2 \frac{G_+^2(\alpha_m)}{2\alpha_m^2} \quad (11)$$

where $G_+(\alpha)$ denotes the 'plus part' of a Wiener-Hopf kernel

$$G(\alpha) = \frac{\Gamma}{\gamma' b (\Gamma + \epsilon_r \gamma' \coth \Gamma b)}$$

where

$$\begin{aligned} \Gamma &= \pm [\alpha_m^2 - (k_0^2 \epsilon_r - \beta_{mn}^2)]^{1/2} \\ &= -i [(k_0^2 \epsilon_r - \beta_{mn}^2 - \alpha_m^2)]^{1/2} \end{aligned}$$

and

$$\begin{aligned}\gamma' &= + [a_m^2 - (k_0^2 - \beta_{mn}^2)]^{1/2} \\ &= -i [(k_0^2 - \beta_{mn}^2) - a_m^2]^{1/2}.\end{aligned}$$

Eqn. (11) is simplified by assuming high reflection coefficient which is possible if $|a_m|^2 \ll (n\pi/b)^2$. A modified form of $G(x)$ leads to the following simplified form for R_{mn} :

$$R_{mn} = (-1) \exp [i(4\pi P_m)^{1/2} (1+i) 0.824 g_0] \quad (12)$$

where the parameter P_m involves the shape factor (a/b) and g_0 involves the thickness and ϵ_r .

The values of α_m and β_{mn} derived¹⁰ by rigorous method are given by

$$\frac{\alpha_m}{k_0} = \frac{\pi}{k_0 b} [P_m (2n + P_m)]^{1/2} \quad (13)$$

$$\frac{\beta_{mn}}{k_0} = \left[\epsilon_r - \frac{\pi (n + P_m)^2}{k_0 b} \right]^{1/2} \quad (14)$$

and are tabulated in Appendix II and are compared with those obtained by trial and experimental method in Appendix III.

The values of $|R_{mn}|$, α_m/k_0 and β_{mn}/k_0 as function of the shape factor a/b are represented graphically in Figs. 4 and 5.

2.4. Scalar functions $\psi_{mn}^{(1)}$, $\psi_{mn}^{(2)}$, $\psi_{mn}^{(3)}$

The scalar potentials in the three regions are given by

$$\begin{aligned}\text{Region 1: } & -a < x < a \\ & 0 < z < b \quad \epsilon_r, \mu_0, \sigma_0\end{aligned}$$

$$\psi_{mn}^{(1)} = C_1 \begin{Bmatrix} \cos \alpha_m x \\ \sin \alpha_m x \end{Bmatrix} \exp(i\beta_{mn}y) \cos\left(\frac{n\pi z}{b}\right); \quad \begin{matrix} m = 1, 3, \dots \\ n = 2, 4, \dots \end{matrix} \quad (15.1)$$

$$\begin{aligned}\text{Region 2: } & a < x < \infty \\ & 0 < z < b \quad \epsilon_r, \mu_0, \sigma_0\end{aligned}$$

$$\psi_{mn}^{(2)} = C_2 \exp(-i\alpha_m x) \exp(i\beta_{mn}y) \cos\left(\frac{n\pi z}{b}\right) \quad (15.2)$$

$$\text{Region 3: } \epsilon_0, \mu_0, \sigma_0$$

$$\psi_{mn}^{(3)} = C_3 \exp(-i\alpha_m x) \exp(i\beta_{mn}y) \exp(i\gamma z) \quad (15.3)$$

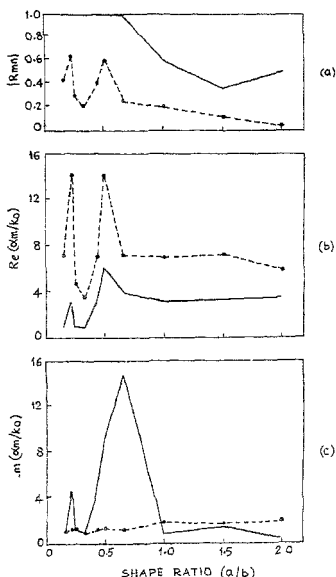


FIG. 4. Variation of $|R_{mn}|$ and a_m with (a/b) .
 (a) $|R_{mn}|$ vs. (a/b) . (b) $\text{Re}(a_m/k_0)$ vs. (a/b) .
 (c) $\text{Im}(a_m/k_0)$ vs. (a/b) .
 $f = 9.375$ GHz, $L = 12.8$ cm, $\epsilon_r = 2.56$
 — Fong (method 1), --- Trial and Expt.
 (Method 2).

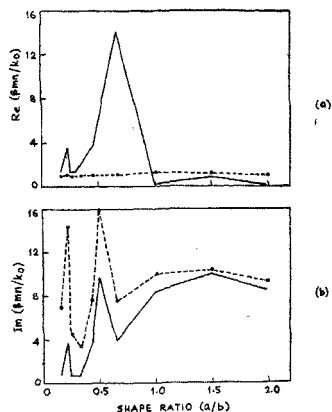


FIG. 5. Variation of β_{mn} with (a/b) .
 (a) $\text{Re}(\beta_{mn}/k_0)$ vs. (a/b) . (b) $\text{Im}(\beta_{mn}/k_0)$ vs. (a/b) .
 $f = 9.375$ GHz, $L = 12.8$ cm, $\epsilon_r = 2.56$
 — Fong (method 1), --- Trial and Expt.
 (Method 2).

where C_1, C_2, C_3 are constants and the propagation constant γ in the z -direction satisfies the relation

$$a_m^2 + \beta_{mn}^2 + \gamma^2 = k_0^2. \quad (15.4)$$

To determine C_1, C_2 and C_3 impose the following boundary conditions

- (i) At $z = 0, z = b$ and $-a < x < a, E_x = 0, E_y = 0$.
- (ii) At $z = b, x > a$, i.e., at the interface between regions 2 and 3, H_x is continuous.
- (iii) At $x = \pm a$, i.e., at the interface between regions 1 and 2 E_x is continuous.

Hence

$$\begin{aligned}
 C_2 &= C_1 \left\{ \frac{\cos \alpha_m a}{\sin \alpha_m a} \right\} \exp(-i\alpha_m a) \\
 C_3 &= C_1 \left\{ \frac{\cos \alpha_m a}{\sin \alpha_m a} \right\} \exp(-i\alpha_m a) e^{-i\gamma b}
 \end{aligned} \tag{15.5}$$

2.5. Field components

Expressing γ_{mn} in different regions in terms of the constant C_1 , the field components for the TM_{mn}^z mode (for $+x$ and $+y$ regions) are obtained as follows:

$$\begin{aligned}
 E_x &= \frac{i}{\omega \epsilon} \left[C_1 \left\{ \frac{\cos \alpha_m a}{\sin \alpha_m a} \right\} \exp(-i\alpha_m a) \exp(-i\gamma b) \right] \\
 &\quad \times (-i\alpha_m) \exp(-i\alpha_m x) \exp(i\beta_{mn} y) (i\gamma) \exp(i\gamma z) \\
 E_y &= \frac{i}{\omega \epsilon} \left[C_1 \left\{ \frac{\cos \alpha_m a}{\sin \alpha_m a} \right\} \exp(-i\alpha_m a) \exp(-i\gamma b) \right] \\
 &\quad \times \exp(-i\alpha_m x) (i\beta_{mn}) \exp(i\beta_{mn} y) (i\gamma) \exp(i\gamma z) \\
 E_z &= \frac{i}{\omega \epsilon} \left[C_1 \left\{ \frac{\cos \alpha_m a}{\sin \alpha_m a} \right\} \exp(-i\alpha_m a) \exp(-i\gamma b) \right] \\
 &\quad \times \{(i\gamma)^2 + k_0^2 \epsilon_r\} \exp(-i\alpha_m x) \exp(i\beta_{mn} y) \exp(i\gamma z) \\
 H_x &= - \left[C_1 \left\{ \frac{\cos \alpha_m a}{\sin \alpha_m a} \right\} \exp(-i\alpha_m a) \exp(-i\gamma b) \right] \\
 &\quad \times \exp(-i\alpha_m x) (i\beta_{mn}) \exp(i\beta_{mn} y) \exp(i\gamma z) \\
 H_y &= \left[C_1 \left\{ \frac{\cos \alpha_m a}{\sin \alpha_m a} \right\} \exp(-i\alpha_m a) \exp(-i\gamma b) \right] \\
 &\quad \times (-i\alpha_m) \exp(-i\alpha_m x) \exp(i\beta_{mn} y) \exp(i\gamma z). \\
 H_z &= 0.
 \end{aligned} \tag{16}$$

In the case of $-x$ and $-y$ regions a plus sign for x variation and a minus sign for the y variation are introduced in the appropriate exponents.

2.6. Experimental study of near field

Several microstrip structures shown in Fig. 6 were made and near field measurements were carried with the help of field sampling probe (Figs. 7-8). Results of near field measurements are presented in Figs. 9, 10 and 11.

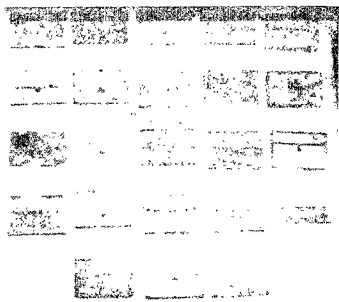


FIG. 6. Microstrip structures used in the experimental study.

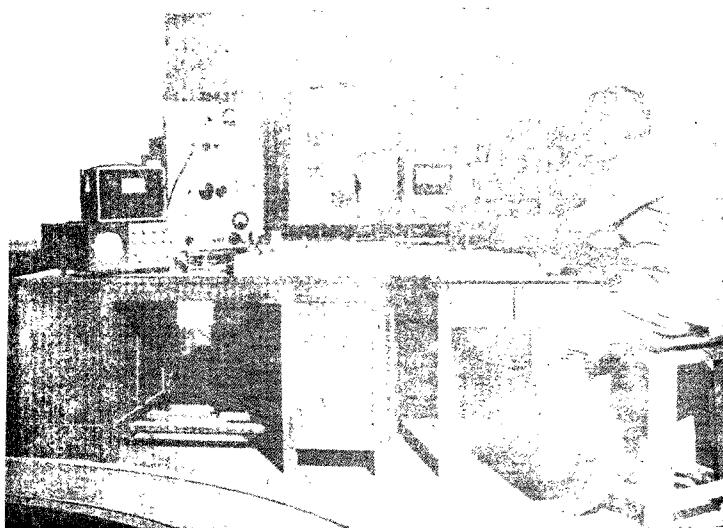


FIG. 7. Experimental set-up for near field measurements.

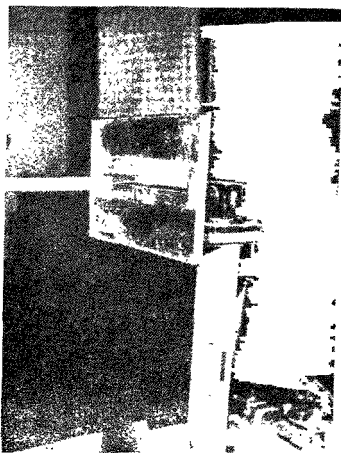


FIG. 8. Monopole probe sampling near the field of the microstrip.

3. Radiation characteristics

3.1. Mechanism of radiation

The derivation of the theory of radiation characteristics requires an understanding of the mechanism of radiation. The microstrip being an open structure, the field at the edges of the strip gets diffracted and induces current at the upper surface of the strip, even if $|R_{\text{in}}| \cong 1$ at $x = \pm a$, i.e., even when the enclosed region acts as a resonator¹¹. For an infinitely thin strip, the currents on the two surfaces may be regarded as continuous, in which case the strip acts as an infinitely thin current filament providing source of radiation.

The effect of the ground plane is to create an image of the infinitely thin strip at $z = -b$, the distance between the strip and the image being $2b$. The radiation field may therefore be considered due to the strip and its image acting as a two-element array (Fig. 12). The radiation pattern of the structure is derived by multiplying the radiation pattern of the strip by the array factor.

The concept of image has been introduced due to the following reasons. Maxwell's equation $\nabla \times \vec{H} = \vec{J} + \partial \vec{D} / \partial t$ shows that the dielectric polarisation acts as an impressed current density. If the polarisation over the cross-section is integrated we get the effective impressed current per unit length of the strip which is proportional to $2/\eta$

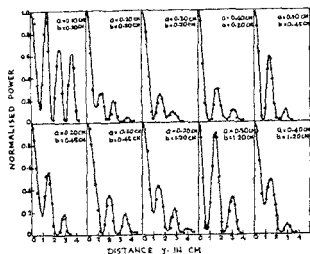


FIG. 9. Measured near field component $|E_z|^2$ vs y (Guide wavelength λ_g) $f = 9.375$ GHz, $L = 12.8$ cm, $\epsilon_r = 2.56$,

$\vec{E} \cdot d\vec{s}$ where η denotes the intrinsic impedance of the dielectric. The factor 2 before the integral sign arises from the positive image of the polarisation currents in the ground plane.¹

The microstrip structure may also be regarded as a grounded dielectric slab excited by an electric line source located within the dielectric plate. If the area of the strip is very small compared to that of the ground plane, then the radiated field may also arise¹² due to the grounded slab.

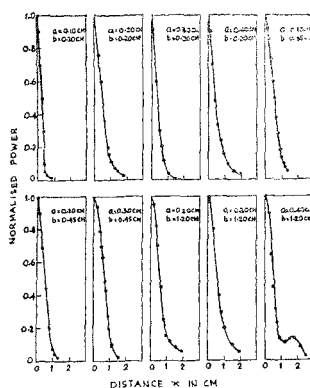


FIG. 10. Experimental field decay in transverse direction, $f = 9.375$ GHz, $L = 12.8$ cm, $\epsilon_r = 2.56$.

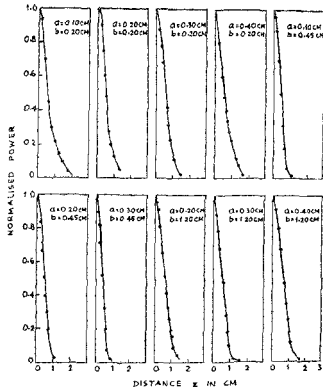


FIG. 11. Experimental variation of $|E_z|^2$ along Z direction over the dielectric surface, $f = 9.375$ GHz, $L = 12.8$ cm, $\epsilon_r = 2.56$.

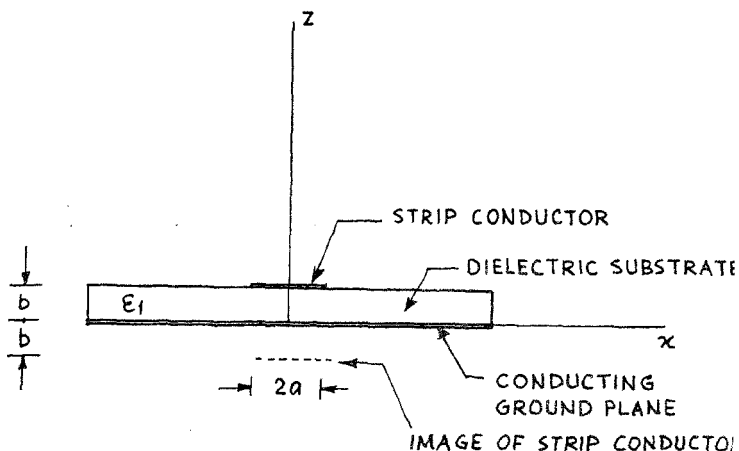


FIG. 12. Cross-section of the microstrip showing the strip and image.

Since it is found that the field decays very sharply inside the dielectric substrate, the radiation due to the grounded dielectric is very small and hence the radiation field is mainly contributed by the strip and its image.

3.2. Theoretical method

The method is based on the angular spectrum¹³ of plane waves. In view of the strip being a conductor, only the tangential components H_x and H_y located in the x - y plane at $z = b$ (Fig. 13) are considered.

3.2.1. Angular spectrum of plane waves

The magnetic field in the aperture plane is given by

$$H(x, y, b) = \frac{k_0^2}{4\pi^2} \int_{-\infty}^{\infty} \int_{-\infty}^{\infty} F(S_1, S_2) \exp [ik_0 (S_1 x + S_2 y + Cb)] dS_1 dS_2 \quad (17)$$

where $F(S_1, S_2)$ is the Fourier transform of $H(x, y, b)$, the aperture plane magnetic field. The Fourier transform is calculated from $H(x, y, b)$ by the inverse relation

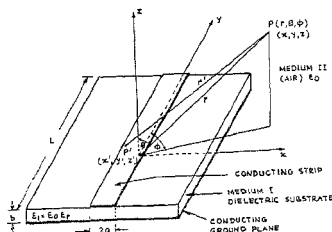


FIG. 13. Geometry of the microstrip antenna for evaluating the radiation fields.

$$F(S_1 S_2) = \int_{-\infty}^{\infty} \int_{-\infty}^{\infty} H(x, y, b) \exp[-ik_0(S_1 x + S_2 y + Cb)] dx dy \quad (18)$$

where

$$S_1 = \sin \theta \sin \phi, \quad S_2 = \sin \theta \cos \phi, \quad (19)$$

$$C = \sqrt{1 - S_1^2 - S_2^2} = \cos \theta.$$

Since the fields are extending over the finite region occupied by the strip and a portion of the dielectric, the boundaries of the finite region may be defined by

$$-a' \leq x' \leq a', \quad -\frac{L}{2} \leq y' \leq \frac{L}{2}$$

where $x' = \pm a'$ are the values of x at which the field strength becomes negligibly small, typically 0.01 times the strength of the field at the centre of the strip.

The limits in eqn. (18) may be split up as extending from ∞ to a' , a' to $-a'$ and $-a'$ to $-\infty$ for the first integral and extending from ∞ to $L/2$, $L/2$ to $-L/2$ and $-L/2$ to $-\infty$ for the second integral.

The contributions from the limits ∞ to a' , $-a'$ to $-\infty$, ∞ to $L/2$ and $-L/2$ to $-\infty$ to the integrals will be negligible and hence these may be ignored. The eqn. (18) may therefore be written as

$$\vec{F}(S_1 S_2) = \int_{-a'}^{a'} \int_{-L/2}^{L/2} \vec{H}(x, y, b) \exp[-ik_0(S_1 x + S_2 y + Cb)] dx dy. \quad (20)$$

The magnetic field at any point (x, y, z) is then given by

$$H(x, y, z) = \frac{k_0^2}{4\pi^2} \int_{-a'}^{a'} \int_{-L/2}^{L/2} F(S_1 S_2) \exp[ik_0(S_1 x + S_2 y + Cb)] dS_1 dS_2. \quad (21)$$

The point of observation (r, θ, ϕ) is redefined by putting $\theta = \theta_0$ and $\phi = \phi_0$. Making these substitutions in eqn. (21) and evaluating the resulting integral by a double application of the stationary phase method (Appendix IV), the magnetic field at the observation point is given by

$$H(x, y, z) = \frac{k_0^2}{4\pi^2} \vec{F}(S_1^0, S_2^0) \frac{2\pi}{k_0 r} e^{ik_0 r} \cos \theta_0 \quad (22)$$

where $F(S_1^0, S_2^0)$ is given by eqn. (20) after substituting $\theta = \theta_0, \phi = \phi_0$. It is therefore seen that from a knowledge of the aperture fields, the radiation fields may be derived.

3.2.2. Evaluation of radiation fields

By using the vector transformation (Appendix V) the electric fields in the spherical polar coordinate system are given by

$$\begin{aligned} E_\theta &= \cos \theta_0 \sin \phi_0 E_x + \cos \theta_0 \cos \phi_0 E_y - \sin \theta_0 E_z \\ E_\phi &= -\cos \phi_0 E_x + \sin \phi_0 E_y. \end{aligned} \quad (23)$$

Since there are two components ($H_{x'}$, $H_{y'}$) on the surface of the strip, only one of them will be considered at a time. Considering the component $H_{y'}$,

$$F_1(S_1^0, S_2^0) = \int_{x'=-a'}^{x'=a'} \int_{y'=-L/2}^{y'=L/2} H_{y'}(x, y, z) \exp[-ik_0(S_1 x' + S_2 y' + Cb)] dx' dy'. \quad (24)$$

Substituting $H_{y'}$, S_1 , S_2 and C into (24) we obtain

$$\begin{aligned} F_1(S_1^0, S_2^0) &= \int_{x'=-a'}^{x'=a'} \int_{y'=-L/2}^{y'=L/2} [K_1(-ia_m) \exp(-ia_m x') \exp(i\beta_{mn} y')] \\ &\quad \times \exp[-ik_0(\sin \theta_0 \sin \phi_0 x' + \sin \theta_0 \cos \phi_0 y' + b \cos \theta_0) \times dx' dy'] \\ &= K_1(-ia_m) \exp(-ik_0 b \cos \theta_0) \int_{x'=-a'}^{x'=a'} \left\{ \exp -i(a_m + k_0 \sin \theta_0 \right. \\ &\quad \times \sin \phi_0) x' \left. \right\} dx' \int_{y'=-L/2}^{y'=L/2} \exp \{i(\beta_{mn} - k_0 \sin \theta_0 \cos \phi_0) y'\} dy' \\ &= K_1(-ia_m) \exp [ik_0 b \cos \theta_0] \left[\frac{e^{i\beta_{mn} a} - 1}{p} + \frac{e^{i\beta_{mn} a} - 1}{q} \right] \\ &\quad \times \left[\frac{e^{i\beta_{mn} L/2} - 1}{s} + \frac{e^{i\beta_{mn} L/2} - 1}{t} \right] \end{aligned} \quad (25)$$

where

$$K_1 = C_1 \left\{ \begin{array}{l} \cos \alpha_m a \\ \sin \alpha_m a \end{array} \right\} \exp(-i \alpha_m a) \exp(-i y b) \quad (26)$$

$$p = -i (\alpha_m - k_0 \sin \theta_0 \sin \phi_0)$$

$$q = -i (\alpha_m + k_0 \sin \theta_0 \sin \phi_0)$$

$$s = i (\beta_{mn} - k_0 \sin \theta_0 \cos \phi_0)$$

$$t = i (\beta_{mn} + k_0 \sin \theta_0 \cos \phi_0) \quad (27)$$

The H_y component at the point of observation is obtained by substituting (25) into (22)

$$\begin{aligned} H_y(x, y, z) &= \frac{k_0^2}{4\pi^2} K_1 (-i \alpha_m) \exp(-i k_0 b \cos \theta_0) \left[\frac{e^{pa'} - 1}{p} + \frac{e^{qa'} - 1}{q} \right] \\ &\quad \times \left[\frac{e^{sL/2} - 1}{s} + \frac{e^{tL/2} - 1}{t} \right] \frac{2\pi i}{k_0 r} e^{ik_0 r} \cos \theta_0 \\ H_y(x, y, z) &= K_2 (-i \alpha_m) \left[\frac{e^{pa'} - 1}{p} + \frac{e^{qa'} - 1}{q} \right] \left[\frac{e^{sL/2} - 1}{s} + \frac{e^{tL/2}}{t} \right] \cos \theta_0 \end{aligned} \quad (28)$$

where

$$K_2 = \left[\frac{k_0^2}{4\pi^2} K_1 e^{ik_0 b \cos \theta_0} \frac{2\pi i}{k_0 r} e^{ik_0 r} \right] \quad (29)$$

Next consider $F_2(S_1^0, S_2^0)$ due to the component H_z'

$$F_2(S_1^0, S_2^0) = \int_{x'=0}^{x'=a'} \int_{y'=-L/2}^{y'=L/2} H_z'(x, y, z) \exp[-ik_0(S_1 x' + S_2 y' + Cb)] dx' dy' \quad (30)$$

Substituting H_z' , S_1 , S_2 and C into (30) we obtain

$$\begin{aligned} &F(S_1^0, S_2^0) \int_{x'=0}^{x'=a'} \int_{y'=-L/2}^{y'=L/2} [-K_1 (i\beta_{mn}) \exp(-i \alpha_m x') \exp(i\beta_{mn} y')] \\ &\quad \times \exp[-ik_0(\sin \theta_0 \sin \phi_0 x' + \sin \theta_0 \cos \phi_0 y' + \cos \theta_0 b)] dx' dy' \\ &= -K_1 (i\beta_{mn}) \exp(-ik_0 \cos \theta_0 b) \int_{x'=0}^{x'=a'} \exp\{-i(\alpha_m + k_0 \sin \theta_0 \sin \phi_0) x'\} dx' \\ &\quad \times \int_{y'=-L/2}^{y'=L/2} \exp\{(i\beta_{mn} - k_0 \sin \theta_0 \cos \phi_0) y'\} dy' \end{aligned}$$

$$F(S_1^0, S_2^0) = -K_1(i\beta_{mn}) \exp(-ik_0 b \cos \theta_0) \left[\frac{e^{pa'} - 1}{p} + \frac{e^{qa'} - 1}{q} \right] \\ \times \left[\frac{e^{sL/2} - 1}{s} + \frac{e^{tL/2} - 1}{t} \right]. \quad (31)$$

The H_z component at the observation point is obtained by substituting (31) into (22). Hence the far field component H_z is given by

$$H_z(x, y, z) = -K_2(i\beta_{mn}) \left[\frac{e^{pa'} - 1}{p} + \frac{e^{qa'} - 1}{q} \right] \left[\frac{e^{sL/2} - 1}{s} \right. \\ \left. + \frac{e^{tL/2} - 1}{t} \right] \cos \theta_0 \quad (32)$$

Hence the electric field components E_x , E_y and E_z at the distant point $p(\tau, \theta, \phi)$ are obtained with the aid of Maxwell's equation

$$E_x = K_2(-i\alpha_m)\eta_0 \cos \theta_0 \left[\frac{\exp[-i(\alpha_m - k_0 \sin \theta_0 \sin \phi_0) a'] - 1}{-i(\alpha_m - k_0 \sin \theta_0 \sin \phi_0)} \right. \\ \left. + \frac{\exp[-i(\alpha_m + k_0 \sin \theta_0 \sin \phi_0) a'] - 1}{-i(\alpha_m + k_0 \sin \theta_0 \sin \phi_0)} \right] \\ \times \left[\frac{\exp[i(\beta_{mn} - k_0 \sin \theta_0 \cos \phi_0) L/2] - 1}{i(\beta_{mn} - k_0 \sin \theta_0 \cos \phi_0)} \right. \\ \left. + \frac{\exp[i(\beta_{mn} + k_0 \sin \theta_0 \cos \phi_0) L/2] - 1}{i(\beta_{mn} + k_0 \sin \theta_0 \cos \phi_0)} \right] \cos \theta_0 \quad (33)$$

$$E_y = -K_2(i\beta_{mn})\eta_0 \cos \theta_0 \left[\frac{\exp[-i(\alpha_m - k_0 \sin \theta_0 \sin \phi_0) a'] - 1}{-i(\alpha_m - k_0 \sin \theta_0 \sin \phi_0)} \right. \\ \left. + \frac{\exp[-i(\alpha_m + k_0 \sin \theta_0 \sin \phi_0) a'] - 1}{-i(\alpha_m + k_0 \sin \theta_0 \sin \phi_0)} \right] \\ \times \left[\frac{\exp[i(\beta_{mn} - k_0 \sin \theta_0 \cos \phi_0) L/2] - 1}{i(\beta_{mn} - k_0 \sin \theta_0 \cos \phi_0)} \right. \\ \left. + \frac{\exp[i(\beta_{mn} + k_0 \sin \theta_0 \cos \phi_0) L/2] - 1}{i(\beta_{mn} + k_0 \sin \theta_0 \cos \phi_0)} \right] \cos \theta_0 \quad (34)$$

$$E_z = -(\tan \theta_0 \sin \phi_0 E_x + \tan \theta_0 \cos \phi_0 E_y). \quad (35)$$

3.2.3. Effect of the ground plane

The strip conductor and its image form a pair of two in-phase radiating elements separated by a distance $2b$ (Fig. 12). The array factor due to this pair is given by

$$A = [1 + e^{i\psi}] \quad (36)$$

where ψ_1 , the phase difference due to the path length difference is given by

$$\psi_1 = 2b k_0 \cos \theta_0. \quad (37)$$

The x -component of the total electric field due to the two-element array formed by the strip and its image is therefore

$$\begin{aligned} E_{T_x} = AE_x = & [1 + \exp(i2b k_0 \cos \theta_0)] K_2(-i\alpha_m) \eta_0 \cos \theta_0 \\ & \times \left[\frac{\exp[-i(\alpha_m - k_0 \sin \theta_0 \sin \phi_0) a'] - 1}{-i(\alpha_m - k_0 \sin \theta_0 \sin \phi_0)} \right. \\ & \left. + \frac{\exp[-i(\alpha_m + k_0 \sin \theta_0 \sin \phi_0) a'] - 1}{-i(\alpha_m + k_0 \sin \theta_0 \sin \phi_0)} \right] \\ & \times \left[\frac{i(\beta_{mn} - k_0 \sin \theta_0 \cos \phi_0) L/2 - 1}{i(\beta_{mn} - k_0 \sin \theta_0 \cos \phi_0)} \right. \\ & \left. \times \frac{\exp[i(\beta_{mn} + k_0 \sin \theta_0 \cos \phi_0) L/2] - 1}{i(\beta_{mn} + k_0 \sin \theta_0 \cos \phi_0)} \right] \cos \theta_0 \end{aligned} \quad (38)$$

Equation (38) represents the radiation pattern in the $\theta_0 - \phi_0$ plane due to the strip and its image.

3.2.4. Radiation pattern in the $\phi_0 = 0^\circ$ plane

For $\phi_0 = 0^\circ$ eqn. (38) yields

$$\begin{aligned} E_{T_x}(\phi_0 = 0^\circ) = & [1 + \exp(i2bk_0 \cos \theta_0)] K_2(-i\alpha_m) \eta_0 \cos \theta_0 \\ & \times \left[\frac{\exp(-i\alpha_m a') - 1}{-i\alpha_m} \frac{\exp(-i\alpha_m a') - 1}{-i\alpha_m} \right] \\ & \times \left[\frac{\exp[i(\beta_{mn} - k_0 \sin \theta_0) L/2] - 1}{i(\beta_{mn} - k_0 \sin \theta_0)} \right. \\ & \left. \times \frac{\exp[i(\beta_{mn} + k_0 \sin \theta_0) L/2] - 1}{i(\beta_{mn} + k_0 \sin \theta_0)} \right] \cos \theta_0. \end{aligned} \quad (39)$$

3.2.4. Numerical computations of radiation patterns

The power radiation patterns in the $\phi_0 = 0^\circ$ plane have been computed with the aid of IBM 360/44 computer for several antennas of different dimensions and are reported in Section 5 (Fig. 19). It is observed that some of the antennas are characterised by only one lobe, whereas antennas A8, A9, and A10 have side lobes. The position of side lobe and its magnitude relative to main lobe vary with shape factor. For example, for antenna A8 which has a shape factor 0.167 (a/b), the side lobe position and relative level are 63° and -17.2 db, respectively, whereas, for antenna A9 having a shape factor $a/b = 0.25$, the position and relative side lobe level are 65° and -15.8 db respectively.

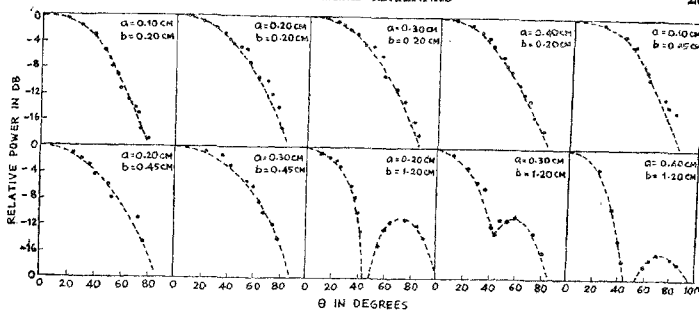


FIG. 14. Experimental radiation patterns in $\phi = 0^\circ$ plane at 9.375 GHz. $L = 12.8$ cm, $\epsilon_r = 2.56$.

3.2.5. Measurement of radiation patterns

The radiation characteristics of several antennas have been measured in an out-door test range and for some antennas in a microwave anechoic chamber. Some of the results are reported in Section 5 (Fig. 19). Experimental radiation patterns obtained at X-band frequencies by using X-Y recorder are reported in Figs. 14 and 15. Analysis of the radiation patterns regarding the position of major and minor lobes, the side lobe level and 3 db-beam width of major lobes have been carried out and is not reported here. The analysis shows some interesting results.

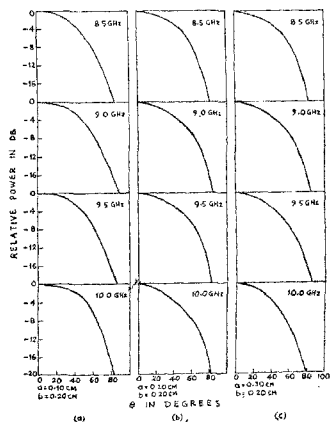


FIG. 15. Experimental radiation patterns in $\phi = 0^\circ$ plane at X-band frequencies (obtained from X-Y recorder) $L = 12.8$ cm, $\epsilon_r = 2.56$.

4. Directivity, gain, radiation efficiency and input impedance characteristics

4.1. Directivity

The total power radiated by the antenna is given by

$$P_T = \int_{\phi=0}^{\phi=2\pi} \int_{\theta=0}^{\theta=\pi} P(\theta, \phi) r^2 \sin \theta \, d\theta \, d\phi \quad (40)$$

where $P(\theta, \phi)$ is given by

$$P(\theta, \phi) = (AE_\theta AH_\phi - AE_\phi AH_\theta) = \left[\frac{E_T^2 \theta + E_T^2 \phi}{\eta_0} \right] \quad (41)$$

where $E_T \theta$ and $E_T \phi$ are given by

$$E_T \theta = \cos \theta \sin \phi AE_x + \cos \theta \cos \phi AE_y - \sin \theta AE_z \quad (42)$$

$$E_T \phi = -\cos \phi AE_x + \sin \phi AE_y \quad (43)$$

$$\begin{aligned} E_T^2 \theta &= [1 + \exp(i2bk_0 \cos \theta)]^2 \left[K_2(-i\alpha_m) \eta_0 \cos \theta \right. \\ &\times \left\{ \frac{\exp[-i(\alpha_m - k_0 \sin \theta \sin \phi) a'] - 1}{-i(\alpha_m - k_0 \sin \theta \sin \phi)} \right. \\ &\left. + \frac{\exp[-i(\alpha_m + k_0 \sin \theta \sin \phi) a'] - 1}{-i(\alpha_m + k_0 \sin \theta \sin \phi)} \right\} \\ &\times \left\{ \frac{\exp[i(\beta_{mn} - k_0 \sin \theta \cos \phi) L/2] - 1}{i(\beta_{mn} - k_0 \sin \theta \cos \phi)} \right. \\ &\left. + \frac{\exp[i(\beta_{mn} + k_0 \sin \theta \cos \phi) L/2] - 1}{i(\beta_{mn} + k_0 \sin \theta \cos \phi)} \right\} \cos \theta \left. \right]^2 \\ &\times \left[\cos \theta \sin \phi - \cos \theta \cos \phi \frac{i\beta_{mn}}{-i\alpha_m} + \sin \theta \left\{ \tan \theta \sin \phi \right. \right. \\ &\left. \left. - \tan \theta \cos \phi \frac{i\beta_{mn}}{-i\alpha_m} \right\} \right]^2. \quad (44) \end{aligned}$$

$$\begin{aligned} E_T^2 \phi &= [1 + \exp(i2bk_0 \cos \theta)]^2 \left[K_2(-i\alpha_m) \eta_0 \cos \theta \right. \\ &\times \left\{ \frac{\exp - [i(\alpha_m - k_0 \sin \theta \sin \phi) a'] - 1}{-i(\alpha_m - k_0 \sin \theta \sin \phi)} \right. \\ &\left. + \frac{\exp - [i(\alpha_m + k_0 \sin \theta \sin \phi) a'] - 1}{-i(\alpha_m + k_0 \sin \theta \sin \theta)} \right\} \\ &\times \left\{ \frac{\exp [i(\beta_{mn} - k_0 \sin \theta \cos \phi) L/2] - 1}{i(\beta_{mn} - k_0 \sin \theta \cos \phi)} \right. \end{aligned}$$

$$\begin{aligned}
 & + \frac{\exp [i(\beta_{mn} + k_0 \sin \theta \cos \phi) L/2] - 1}{i(\beta_{mn} + k_0 \sin \theta \cos \phi)} \cos \theta \Big]^2 \\
 & \times \left[\cos \phi + \frac{i\beta_{mn}}{-ia_m} \sin \phi \right]^2
 \end{aligned} \tag{45}$$

The total power radiated by the antenna is given by

$$\begin{aligned}
 P_t = & \int_{\phi=0}^{2\pi} \int_{\theta=0}^{\pi} [(1 + \exp(i2bk_0 \cos \theta))^2] \left[k_2 (-ia_m) \cos \theta \right. \\
 & \times \left\{ \frac{\exp[-i(a_m - k_0 \sin \theta \sin \phi) a'] - 1}{-i(a_m - k_0 \sin \theta \sin \phi)} \right. \\
 & \left. \left. + \frac{\exp[-i(a_m + k_0 \sin \theta \sin \phi) a'] - 1}{-i(a_m + k_0 \sin \theta \sin \phi)} \right\} \right. \\
 & \times \frac{\exp - i(\beta_{mn} - k_0 \sin \theta \cos \phi) L/2 - 1}{i(\beta_{mn} - k_0 \sin \theta \cos \phi)} \\
 & \left. \left. + \frac{\exp [i(\beta_{mn} + k_0 \sin \theta \cos \phi) L/2] - 1}{i(\beta_{mn} + k_0 \sin \theta \cos \phi)} \right\} \cos \theta \right]^2 \\
 & \times \left[\cos \theta \sin \phi - \cos \theta \cos \phi \left(\frac{i\beta_{mn}}{-ia_m} \right) + \sin \theta \left(\tan \theta \sin \theta - \tan \theta \cos \theta \right) \right. \\
 & \left. \times \left(\frac{i\beta_{mn}}{-ia_m} \right) \right]^2 + \left(\cos \theta + \left(\frac{i\beta_{mn}}{-ia_m} \right) \sin \phi \right)^2 \Big] r^2 \sin \theta \, d\theta \, d\phi.
 \end{aligned} \tag{46}$$

The usual definition of directivity is

$$\text{Directivity} = \frac{4\pi P(0, 0)}{\int_{\theta=0}^{\pi} \int_{\phi=0}^{2\pi} P(\theta, \phi) r^2 \sin \theta \, d\theta \, d\phi} \tag{47}$$

without taking into account heating losses or reflection losses. The direction of peak radiation is given by $\theta = 0^\circ$, $\phi = 0^\circ$, which is confirmed by experiment.

Since

$$\begin{aligned}
 (E_{r2})^2 = P(0, 0)_{\max} = & (1 + e^{i2bk_0})^2 \left[K(-ia_m) \eta_0 \left(\frac{2}{-ia_m} \right) \right. \\
 & \left. \times \left\{ \exp(-ia_m a') - 1 \right\} \left(\frac{2}{i\beta_{mn}} \right) \left\{ \exp \left(i\beta_{mn} \frac{L}{2} \right) - 1 \right\} \right]^2
 \end{aligned} \tag{48}$$

where

$$K = \frac{k_0^2}{4\pi^2} K_1 e^{-ia_m} \frac{2\pi i}{k_0 r} e^{i2k_0 r}$$

The directivity D in the $\phi = 0^\circ$ plane is therefore

$$D = \frac{P(0, 0)_{\max}}{P_T/4\pi} \quad (49)$$

which has been computed for antennas with different shape factors by using appropriate values of α_m and β_m . It is found that D varies between 7.2 db to 9.77 db and is higher for antennas having smaller a/b values.

4.2. Gain

The gain of the microstrip antennas has been determined by comparison with a standard pyramidal horn with a gain of 20.6 db in the antenna test range.

The expression for the gain G_0 of the test antenna in terms of the reference antenna is

$$G_0 = 20.6 + 10 \log(P_T/P_r) \quad (50)$$

where P_T and P_r denote the maximum power radiated by the test and reference antennas respectively, the input power to both of them being the same.

Measurement of gain shows that G_0 varies between 5.1 db to 8.3 db with shape factor at $f = 9.375$ GHz. For the same antennas gain varies with different frequencies over the X-band. Some of the results are reported in Table I.

Table I

Experimental gain at X-band frequencies in the $\phi = 0^\circ$ plane.

$$L = 12.8 \text{ cm}, \quad \epsilon_r = 2.56.$$

Antenna	a/b	Gain (db) at X-band frequencies (GHz)			
		8.50	9.0	9.5	10.0
A1	0.5	4.0	4.0	4.0	3.0
A6	0.44	3.5	5.5	4.0	3.0
A10	0.338	6.5	8.5	8.5	6.5

4.3. Radiation efficiency (η_R)

It is defined as

$$\eta_R = \frac{\text{Radiated power } P_R}{\text{Input power } P_{in}}$$

where

$$P_{in} = P_R + P_L = P_R + P_d + P_C \quad (51)$$

where the dielectric loss P_d arises due to the substrate having a finite value of $\tan \delta$, and the ohmic loss P_C arises due to the finite conductivity of the strip and the ground plane.

Since the attenuation constant α of the microstrip is defined as

$$\alpha = P_L / 2P(Z) = \frac{P_C + P_d}{2P(Z)} \quad (52)$$

the radiation efficiency is given by

$$R_1 = \frac{P_R}{2\alpha P(Z) + P_R} \quad (53)$$

The discontinuity at the antenna aperture gives rise to mismatch loss. Hence, in general $P_R < P(Z)$ at the antenna aperture. If, however, the mismatch is small and ignored, then

$$P(Z) \simeq P_R \quad (54)$$

Hence,

$$\eta_{R_1} = \frac{1}{1 + 2\alpha} \quad (55)$$

4.3.1. Dielectric loss (α_d)

The dielectric loss can be calculated from the following relation¹⁴ which assumes that the propagating mode is TEM

$$\frac{\partial U}{\partial \epsilon_1} = \frac{U_1}{\epsilon_1} \quad (56)$$

Equation (56) states that the partial derivative of the total electric field energy U of the microstrip with respect to the relative dielectric constant ϵ_1 of the substrate is given by the ratio of the electric field energy U_1 stored in the dielectric and ϵ_1 .

The dielectric attenuation is given by¹⁵

$$\alpha_d = \frac{20\pi}{\ln(10)} \frac{q \tan \delta}{\lambda} \quad (57)$$

where q is the filling factor given by

$$q = \frac{1}{1 + \frac{F-1}{\epsilon_r(F+1)}} \quad (58)$$

and

$$F(2a, b) = \left(1 + \frac{10b}{2a}\right)^{1/2}$$

4.3.2. Conductor loss (α_c)

The expression for α_c (db/cm) is given by^{14,16}

$$\alpha_{c1} = \left(\frac{R_s}{Z_0 b}\right) \left(\frac{8 \cdot 68}{2\pi}\right) \left[1 - \left(\frac{2a}{4b}\right)^{2.7}\right] \left[1 + \frac{b}{2a}\right] \text{ db/cm}$$

for $\frac{1}{2\pi} < \frac{2a}{b} \leq 2$ (59)

and

$$\alpha_{c2} = \left(\frac{R_s}{Z_0 b}\right) \frac{8 \cdot 68}{\left[\frac{2a}{b} + \frac{2}{\pi} \ln \left\{2\pi e \left(\frac{2a}{2b} + 0 \cdot 94\right)\right\}\right]} \left[\frac{2a}{b} + \frac{2a/\pi b}{2b + 0 \cdot 94}\right] \times \left[1 + \frac{b}{2a}\right] \text{ for } 2 \leq 2a/b$$
 (60)

where the strip conductor is assumed to be infinitely thin and

$$R_s = 8 \cdot 26 \times 10^{-3} \sqrt{f \Omega} \text{ (for Cu)}$$

f is in GHz.

The characteristic impedance Z_0 of the microstrip line is given by¹⁶

$$Z_0 = \frac{377b}{2a \sqrt{\epsilon_r} \left[1 + 1 \cdot 735 \epsilon_r^{-0.0724} \left(\frac{2a}{b}\right)^{-0.650}\right]}$$
 (61)

Since eqns. (59) and (60) have a limited range of operation with regard to $2a/b$, it is observed that whereas most of the antennas are covered by eqn. (59) in the calculation of conductor loss, eqn. (60) must be used for antennas A_3 and A_4 .

4.3.3. Comparison of radiation efficiencies

The radiation efficiencies η_{R_1} (eqn. 55), η_{R_2} defined by

$$\eta_{R_2} = \frac{G_0}{D}$$
 (62)

and η'_{R_2} which includes mismatch loss determined by v.s.w.r. measurements in addition to α_0 and α_d are compared in Table II. ρ is the reflection coefficient computed from v.s.w.r. data which are not reported.

Table II

Comparison of η_{R_1} , η'_{R_1} and η_{R_2}

$f = 9.375$ GHz, $L = 12.8$ cm, $\epsilon_r = 2.56$, $\tan \delta = .005$ (substrate)

Antennas	$\alpha_\theta + \alpha_d$ (db)	Mismatch loss (db) - 10 log (1 - ρ^2)	Total loss α (ncpers)	$\eta_{R_1}\%$	$\eta_{R_2}\%$	$\eta'_{R_1}\%$
A1	0.637	0.045	0.078	85.33	77.0	86.5
A2	0.737	0.055	0.091	84.39	75.0	84.5
A3	0.766	0.025	0.091	83.83	73.0	84.5
A4	0.801	0.075	0.100	83.16	76.39	83.4
A5	0.661	0.040	0.080	85.88	81.50	86.3
A6	0.663	0.035	0.081	85.84	78.33	86.0
A7	0.667	0.030	0.0801	85.76	81.50	86.3
A8	0.620	0.020	0.0736	86.70	85.0	87.6
A9	0.622	0.033	0.075	86.66	82.0	87.0
A10	0.636	0.020	0.075	86.38	84.5	87.0

It is observed that there is difference in the three values of η_R and also between $\eta'_{R_1} \sim \eta_{R_1}$ and $\eta_{R_2} \sim \eta_{R_2}$. This is due to the fact that $\eta'_{R_1} \sim \eta_{R_1}$ is computed by considering mismatch at the input of the antenna, whereas, $\eta_{R_1} \sim \eta_{R_2}$ is obtained by considering mismatch at the antenna aperture.

4.3.4. Input impedance

The input impedance at the coaxial plug termination fitted to the microstrip structure for the purpose of excitation is measured with the help of a slotted line and computed from the v.s.w.r. and shift in the first position of minima using a Smith chart. The variation of input impedance normalised with respect to the characteristic impedance Z of the R651/U type rectangular waveguide for antennas A1-A10 are plotted in Fig. 16.

5. Discussion and conclusions

5.1. Guided-wave characteristics

We will call Fong's method and the trial and experimental method as the first and the second method respectively.

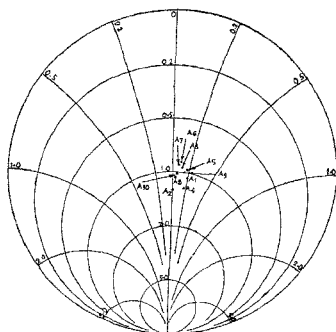


FIG. 16. Normalised input impedance of microstrip antennas.

5.1.1. Propagation coefficients (α_m and β_{mn})

The nature of variation of $\text{Re}(\beta_{mn}/k_0)$ with respect to a/b and also the difference in magnitude according to the two methods may be ascribed to the method of approach in deriving the two theories. In the first method R_{mn} has been assessed so as to fit in the experimental value of λ_g with that of the theory whereas the first method assumes *a priori* $R_{mn} \approx 1$.

The high value of $\text{Im}(\beta_{mn}/k_0)$ suggests loss of energy by radiation. The peak values of $\alpha_{mn}(k_0)$ indicate high rate of decay of the field in the x -direction.

5.1.2. Reflection coefficient (R_{mn})

$|R_{mn}| \approx 1$ up to $a/b = 0.6$ (1st method), whereas $|R_{mn}|$ shows definite maxima and minima within the range $a/b = 0.6$. The minima corresponds to the loss of energy in the x -direction.

5.1.3. Guide wavelength (λ_g)

Smaller values of λ_g corresponding to $(a/b) \geq 1.0$ indicate greater concentration of energy in the microstrip. Larger values of λ_g for $(a/b) < 1.0$ indicate loss of energy by radiation (Fig. 17).

A comparative study of theoretical and experimental values of λ_g (Fig. 17) reveals the purity (which depends on a/b) of TM modes except for $a/b = 0.9$ and $a/b = 0.66$ where the diffraction effect is probably predominant and might contaminate the TM_{11} and TM_{21} modes.

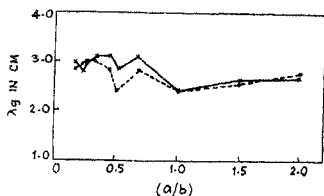


FIG. 17. Variation of guide wavelength λ_g with shape ratio (a/b) . - - - Experiment, — Calculated (Second method)

5.1.4. Purity of TM mode

The purity of modes and hence the method of excitation is justified by the exponential nature of decay characteristics (Fig. 18) for all the microstrips except for A10 where a peak appears at $x = 1.8$ cm away from the centre of the strip. There is also fairly close agreement between the theoretical results calculated by the second method and the experimental results. Since the value of $|R_{\text{min}}|$ is more realistic from the practical point of view the second method is used.

5.1.5. Field supported by the substrate

The region bounded by the strip and the ground plane is open at $x = \pm a$, consequently the field extends beyond $x = \pm a$. In the z -direction, however, the field decays exponentially.

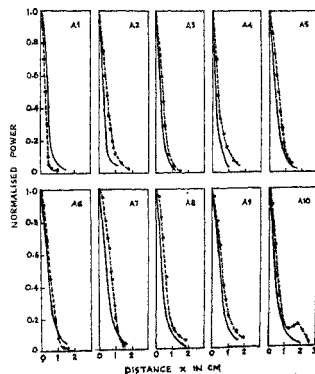


FIG. 18. Variation of $|E_x|^2$ in transverse direction. $f = 9.375$ GHz, $L = 12.8$ cm, $\epsilon_r = 2.56$
— Theory, - - - Expt.

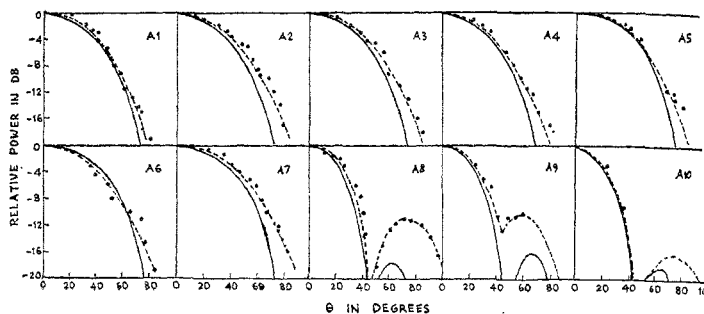


Fig. 19. Radiation patterns in $\phi_0 = 0^\circ$ plane at 9.375 GHz. $L = 12.8$ cm, $\epsilon_r = 2.56$,
 — Theory — — Expt.

5.2. Radiation characteristics

Figures 19 and 20 present comparative studies of theoretical and experimental radiation patterns and beam widths respectively. It is observed that the antennas A1–A7 are characterised by a single broad lobe but the antennas A8–A10 have side lobes the magnitudes of the later relative to the major lobe differ between theory and experiment (Table III).

The single lobe characteristics at X-band for most of the antennas at different frequencies except that of A10 are maintained (Table IV). The frequency dependence of the 3-dB beam width for some of the antennas are reported in Table V.

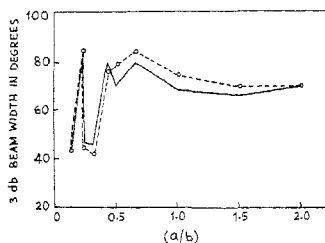


Fig. 20. Variation in 3 dB beam width for different shape factor (a/b).
 $f = 9.375$ GHz, $L = 12.8$ cm, $\epsilon_r = 2.56$.
 — Calculated, — — Experiment.

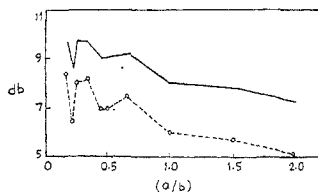


Fig. 21. Gain, directivity characteristics for different shape factor (a/b).
 $f = 9.375$ GHz, $L = 12.8$ cm, $\epsilon_r = 2.56$.
 — Directivity, — — Gain.

Table III

Theoretical and experimental side lobe levels

 $f = 9.375$ GHz, $L = 12.8$ cm, $\epsilon_r = 2.56$

Antenna	Side lobe level		Difference in side lobe level
	Theo.	Expt. db	
A8	-17.2	-11.0	6.2
A9	-15.8	-10.5	5.3
A10	-17.9	-15.9	2

Table IV

Position of side lobe and its relative height compared to the major lobe at X-band frequencies. $L = 12.8$ cm, $\epsilon_r = 2.56$.

Antenna	Shape factor (a/b)	8.5 GHz		9.5 GHz	
		Position of side lobe	Relative height compared to major lobe	Position of side lobe	Relative height compared to major lobe
A10	0.33	75°	-10 db	75°	-15 db

Table V

Variation of 3 db beam width at spot frequencies in the X-band with respect to those at 9.375 GHz, $L = 12.8$ cm, $\epsilon_r = 2.56$.

Antenna	Shape factor (a/b)	Beam width variation compared to 9.375 GHz			
		8.5 GHz	9.0 GHz	9.5 GHz	10.0 GHz
A1	0.5	+6°	+14°	+18°	+18°
A2	1.0	+2°	+2°	+8°	-4°
A3	1.5	+8°	+4°	-2°	-2°
A4	2.0	-8°	-12°	+12°	+32°
A6	0.44	-24°	-20°	-8°	+16°
A10	0.33	-4°	+4°	+16°	+30°

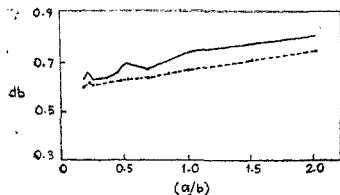


FIG. 22. Microstrip losses for different shape factor (a/b). $f = 9.375$ GHz, $L = 12.8$ cm, $\epsilon_r = 2.56$.
 --- Dielectric Loss, — Total loss (Dielectric + Conductor)

The appearance of side lobes for A8-A10 is possibly due to the increased separation between the strip and its image and hence greater path length difference from $P(r, \theta, \phi)$.

5.3. Directivity, gain, radiation efficiency and input impedance characteristics

5.3.1. Directivity and gain

Gain and directivity characteristics (Fig. 21) as function of a/b show the sensitivity for $a/b < 0.5$ which dictates the requirement of using more accurate fabrication technique. Gain variation at spot frequencies for some antennas are reported in Table VI. The gain appears to be maximum at 9.375 GHz.

5.3.2. Radiation efficiency

Figure 22 shows the variation of dielectric loss and total loss (dielectric + conductor) as a function of a/b . The radiation efficiencies η_{R_1} and η_{R_2} as a function of (a/b) are shown in Fig. 23. The difference between η_{R_2} and η_{R_1} (Fig. 24) accounts for the reduction in radiation efficiency due to the mismatch loss at the antenna aperture.

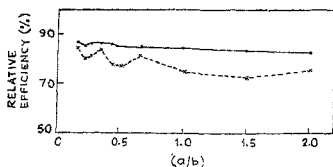


FIG. 23. Radiation efficiency for different shape factor a/b .

$f = 9.375$ GHz, $L = 12.8$ cm, $\epsilon_r = 2.56$,

— η_{R_1} , --- η_{R_2} .

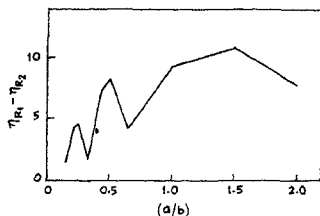


FIG. 24. $\eta_{R_1} - \eta_{R_2}$ for different shape factor (a/b).

Table IV

Variation of gain at spot frequencies in X-band as compared to the gain at 9.375 GHz.

Antenna	Difference in gain w.r.t. 9.375 GHz			
	8.5 GHz	9.0 GHz	9.5 GHz	10.0 GHz
A1	-3.0	-3.0	-3.0	-4.0
A6	-3.0	-1.0	-2.5	-3.5
A10	-1.7	0.3	0.3	-1.7

5.3.3. Input impedance

The input impedance of the microstrip along with the coaxial feed as seen by a slotted section has been measured. The real and imaginary part of the input impedance varying with a/b (as reported earlier) shows that the variation is more rapid for $a/b < 1.0$. The matching between the coaxial feed and the microstrip has been achieved experimentally by adjusting the length of the tapered strip between the feed and the strip radiator.

5.4. Conclusions

- (i) The radiation theory on the basis of two-element array formed by the strip and its image is well justified.
- (ii) The coaxial method of exciting pure TM wave is justified.
- (iii) Higher gain/directivity can be attained with strip of small width and dielectric substrate of small thickness, keeping a/b ratio small.
- (iv) The maximum radiation efficiency is about 87% for small values of a/b .
- (v) The 3-dB beam width is generally high.

It is believed that the major contributions of the investigations are:

- (i) Radiation theory based on the concept of current strip and its image.
- (ii) Estimation of radiation efficiency.
- (iii) Near field analysis.

References

1. LEWIN, L. Radiation from discontinuities in strip lines, *Proc. IEE*, 1960, Part C, **107**, 163-170.
2. DENLINGER, J. Radiation from microstrip resonators, *IEEE Trans. MTT*, 1969, **17**, 235-236.
3. MUNSON, R. E. Conformal microstrip antennas and microstrip phased arrays, *IEEE Trans. A.P.*, 1974, **22**, 74-78.

4. HOWELL, J. Q. Microstrip antennas, *IEEE Trans.*, A.P. 1975, **23**, 90-93.
5. CHATTERJEE, R. AND GANESAN, N. S. Microstrip antennas at microwave frequencies, *Proc. IEE-IERE* 1977, **15**, 103-110.
6. CHATTERJEE, R. AND GANESAN, N. S. Microstrip antenna, *Sixth Colloquium on Microwave Communications*, Budapest, Hungary, September 1978.
7. RAJ MITTRA AND TATSUO ITOH *Advances in Microwaves*, 1974, **8**, 67-141.
8. WEISS, J. A. *Advances in Microwaves*, 1974, **8**, 295-320.
9. ARDITE, M. *IRE Trans. MTT*, 1955, **3**, 31-56.
10. FONG, T. T. AND SHUNG-WU LEE Modal analysis of a planar dielectric strip waveguide to mm wave integrated circuits, *IEEE Trans. MTT*, 1974, **22**, 776-783.
11. VAINSHTEIN, L. A. *Soviet Physics, JETP*, 1963, **17**, 709-719.
12. COLLIN, R. E. AND ZUCKER, F. *Antenna Theory*, Part 2, Ch. 21, 1921, McGraw-Hill, New York.
13. BOOKER, H. C. AND CLEMMOW, P. C. The concept of an angular spectrum of plane waves and its relation to that of polar diagram and aperture distribution, *Proc. IEE, Pt. III*, 1950, **97**, 11-17.
14. SCHNEIDER, M. V. Dielectric loss in integrated microwave circuits, *Bell. Sys. Tech. Jour.*, 1969, **48**, 2325-2332.
15. CARLTON H. WALTER *Travelling Wave Antennas*, Ch. 6, McGraw-Hill, 1965.
16. WHEELER, H. A. Formulas for the skin effect, *Proc. IRE*, 1942, **30**, 412-424.
17. SOBOL, H. Extending IC Technology to Microwave Equipment, *Electronics*, 1967, **40**, 112-124.
18. MAX BORN AND EML WOLF *Principles of Optics*, Third edition (revised), Appendix III, Pergamon Press, 1965.

Appendix I

Microstrip specifications

$$\epsilon_r = 2.56, \quad \tan \delta = 0.005, \quad L = 12.8 \text{ cm.}$$

Structure No.	a in cm	b in cm	a/b
A1	0.10	0.20	0.50
A2	0.20	0.20	1.0
A3	0.30	0.20	1.50
A4	0.40	0.20	2.0
A5	0.10	0.45	0.22
A6	0.20	0.45	0.445
A7	0.30	0.45	0.666
A8	0.20	1.20	0.167
A9	0.30	1.20	0.25
A10	0.40	1.20	0.33

Appendix II

Values of normalised α_m/k_0 , β_{mn}/k_0 and $|R_{mn}|$ calculated from Fong's equations

Structure No.	a in cm	b in cm	$ R_{mn} $	Mode No.		α_m/k_0	β_{mn}/k_0
				m	n		
A1	0.10	0.20	1.0	1	1	6.079 - i9.354	7.188 + i9.71
A2	0.20	0.20	0.60	1	1	3.075 - i0.667	0.24 + i8.39
A3	0.30	0.20	0.368	2	1	6.425 - i1.524	0.973 + i10.066
A4	0.40	0.20	0.526	2	1	3.562 - i0.436	0.18 + i8.60
A5	0.10	0.45	1.0	1	1	3.036 - i4.663	3.70 + i3.823
A6	0.20	0.45	1.0	1	1	3.036 - i4.663	3.70 + i3.82
A7	0.30	0.45	1.0	2	1	3.859 - i14.676	14.24 + i3.97
A8	0.20	1.20	1.0	1	1	0.854 - i1.113	1.34 + i0.71
A9	0.30	1.20	1.0	1	1	0.854 - i1.113	1.34 + i0.71
A10	0.40	1.20	1.0	1	1	0.854 - i1.113	1.34 + i0.71

Appendix III

Comparison of α_m , β_{mn} and $|R_{mn}|$. $f = 9.375$ GHz

Structure No.	α_m/k_0		β_{mn}/k_0		$ R_{mn} $	
	Fong's method	Trial method	Fong's method	Trial method	Fong's method	Trial method
A1	6.08 - i9.35	14.0 - i1.26	7.19 + i9.71	1.10 + i16.0	1.0	0.60
A2	3.07 - i0.67	6.98 - i1.96	0.24 + i8.39	1.325 + i10.04	0.60	0.21
A3	6.42 - i1.52	7.3 - i1.74	0.97 + i10.07	1.20 + i10.62	0.368	0.12
A4	3.56 - i0.44	5.84 - i2.00	0.18 + i8.60	1.17 + i9.40	0.526	0.04
A5	3.04 - i4.66	14.0 - i1.142	3.70 + i3.82	1.12 + i14.3	1.0	0.63
A6	3.04 - i4.66	7.0 - i1.125	3.70 + i3.82	1.03 + i7.65	1.0	0.41
A7	3.86 - i14.68	7.3 - i1.11	14.24 + i3.97	1.04 + i7.95	1.0	0.26
A8	0.85 - i1.11	7.0 - i1.045	1.34 + i0.71	1.055 + i6.94	1.0	0.43
A9	0.85 - i1.11	4.65 - i1.025	1.34 + i0.71	1.045 + i4.56	1.0	0.29
A10	0.85 - i1.11	3.46 - i0.98	1.34 + i0.71	1.015 + i3.40	1.0	0.21

Appendix IV

Integration by the Stationary Phase Method¹⁸

Consider the general expression for the magnetic field given by eqn. (22), this may be rewritten for any component, say H_x as

$$H_x(x, y, z) = \int_{-\infty}^{\infty} \int_{-\infty}^{\infty} F(S_1 S_2) \exp[ik_0(S_1 x + S_2 y + Cz)] dS_1 dS_2 \quad (\text{A.1})$$

When $k_0 r \gg 1$, the exponential factor is a rapidly changing function of S_1 and S_2 and the principal contribution to H arises from the stationary phase region. Let

$$\theta = \theta_0, \quad \phi = \phi_0 \quad (\text{A.2})$$

be the point of observation. Then

$$\begin{aligned} x &= r \sin \theta_0 \sin \phi_0 \\ y &= r \sin \theta_0 \cos \phi_0 \\ z &= r \cos \theta_0 \end{aligned} \quad (\text{A.3})$$

the exponential factor in eqn. (A.1) will therefore be given by

$$\begin{aligned} S_1 x + S_2 y + Cz &= r [\sin \theta \sin \phi \sin \theta_0 \sin \phi_0 + \sin \theta \cos \phi \sin \theta_0 \cos \phi_0 + \cos \theta \cos \theta_0] \\ &= r [\sin \theta \sin \theta_0 \cos(\phi - \phi_0) + \cos \theta \cos \theta_0] \end{aligned} \quad (\text{A.4})$$

dS_1 and dS_2 are given by $J d\theta d\phi$ where J is the Jacobian given by

$$J = \left| \frac{dS_1}{d\theta} \frac{dS_2}{d\phi} - \frac{\partial S_1}{\partial \phi} \frac{\partial S_2}{\partial \theta} \right|.$$

Hence

$$\begin{aligned} J &= | -\cos \theta \sin \phi \sin \theta \sin \phi - \sin \theta \cos \phi \cos \theta \cos \phi | \\ &= | \cos \theta \sin \theta \sin^2 \phi + \sin \theta \cos \theta \cos^2 \phi | \\ &= | \sin \theta \cos \theta |. \end{aligned} \quad (\text{A.5})$$

Equation (A.1) may therefore be rewritten with the appropriate substitutions to give

$$\begin{aligned} H_0(x, y, z) &= \frac{k_0^2}{4\pi^2} \iint F(S_1 S_2) \exp \{ ik_0 r [\sin \theta \sin \theta_0 \cos(\phi - \phi_0) \\ &\quad \mp \cos \theta \cos \theta_0] \} \sin \theta \cos \theta d\theta d\phi \end{aligned} \quad (\text{A.6})$$

denoting the exponential factor in eqn. (A.6) by $f(\theta, \phi)$

$$f(\theta, \phi) = \sin \theta \sin \theta_0 \cos(\phi - \phi_0) + \cos \theta \cos \theta_0. \quad (\text{A.7})$$

At the critical points

$$\frac{\partial f}{\partial \theta} = 0; \quad \frac{\partial f}{\partial \phi} = 0. \quad (\text{A.8})$$

Hence

$$\frac{\partial f}{\partial \phi} = -\sin \theta \sin \theta_0 \sin(\phi - \phi_0) = 0$$

this will be true for

$$\phi = \phi_0. \quad (\text{A.9})$$

Next

$$\frac{\partial f}{\partial \theta} = \cos \theta \sin \theta_0 \cos(\phi - \phi_0) - \sin \theta \cos \theta_0 = 0$$

i.e.,

$$\cos \theta \sin \theta_0 = \sin \theta \cos \theta_0.$$

Hence

$$\cot \theta = \cot \theta_0.$$

Hence

$$\theta = \theta_0. \quad (\text{A.10})$$

Thus eqn. (A.6) may be written as

$$H_y(x, y, z) = \frac{k_0^2}{4\pi^2} F(S_1^0, S_2^0) \frac{e^{i\theta_0 z}}{k_0 r} \frac{2\pi i \sin \theta_0 \cos \theta_0}{(\alpha_1 \beta_1 - \gamma_1^2)^{1/2}} \quad (\text{A.11})$$

where

$$\alpha_1 = \frac{\partial^2 f}{\partial \theta^2}, \quad \beta_1 = \frac{\partial^2 f}{\partial \phi^2}, \quad \gamma_1 = \frac{\partial^2 f}{\partial \theta \partial \phi} \quad (\text{A.12})$$

all evaluated at (θ_0, ϕ_0) and

$$S_1^0 = \sin \theta_0 \sin \phi_0; \quad S_2^0 = \sin \theta_0 \cos \phi_0 \quad (\text{A.13})$$

proceeding to evaluate α_1 , β_1 and γ_1

$$\begin{aligned} \alpha_1 &= \left. \frac{\partial^2 f}{\partial \theta^2} \right|_{(\theta_0, \phi_0)} \\ &= -\sin \theta \sin \theta_0 \cos(\phi - \phi_0) - \cos \theta \cos \theta_0 \end{aligned}$$

at

$$\theta = \theta_0, \quad \phi = \phi_0.$$

∴ The stationary phase point is $(\theta = \theta_0, \phi = \phi_0)$ which is the same as the point of observation

$$a_1 = -\sin^2 \theta_0 - \cos^2 \theta_0 = -1. \quad (\text{A.14})$$

Similarly,

$$\begin{aligned} \beta_1 &= \left. \frac{\partial^2 f}{\partial \phi^2} \right|_{(\theta_0, \phi_0)} \\ &= -\sin \theta_0 \sin \theta_0 \cos(\phi_0 - \phi_0) = -\sin^2 \theta_0 \end{aligned} \quad (\text{A.15})$$

$$\begin{aligned} \gamma_1 &= \left. \frac{\partial^2 f}{\partial \theta \partial \phi} \right|_{(\theta_0, \phi_0)} \\ &= -\cos \theta_0 \sin \theta_0 \sin(\phi_0 - \phi_0) = 0. \end{aligned} \quad (\text{A.16})$$

Hence

$$\frac{1}{\sqrt{a_1 \beta_1 - \gamma_1^2}} = \frac{1}{\sqrt{\sin^2 \theta_0}} = \frac{1}{\sin \theta_0}.$$

Equation (A.11) is therefore reduced to

$$H_y(x, y, z) = \frac{k_0^2}{4\pi^2} F(S_1^0, S_2^0) \frac{2\pi i}{k_0 r} e^{4i\theta_0 r} \cos \theta_0. \quad (\text{A.17})$$

The method described above is quite general in nature and has been worked out using the H_y component as an example.

Appendix V

Vector transformations

$$\begin{pmatrix} i_r \\ i_\theta \\ i_\phi \end{pmatrix} = \begin{pmatrix} \sin \theta \sin \phi & \sin \theta \cos \phi & \cos \theta \\ \cos \theta \sin \phi & \cos \theta \cos \phi & -\sin \theta \\ -\cos \phi & \sin \phi & 0 \end{pmatrix} \begin{pmatrix} i_x \\ i_y \\ i_z \end{pmatrix}$$

$$\begin{pmatrix} i_x \\ i_y \\ i_z \end{pmatrix} = \begin{pmatrix} \sin \theta \sin \phi & \cos \theta \sin \phi & -\cos \phi \\ \sin \theta \cos \phi & \cos \theta \cos \phi & \sin \phi \\ \cos \theta & -\sin \theta & 0 \end{pmatrix} \begin{pmatrix} i_r \\ i_\theta \\ i_\phi \end{pmatrix}$$